Draft version September 27, 2018
Typeset using LaTeX **twocolumn** style in AASTeX62

Predicting the Rossby number in convective experiments

Evan H. Anders,[1,2] Cathryn M. Manduca,[2] Benjamin P. Brown,[1,2] Jeffrey S. Oishi,[3] and Geoff Vasil[4]

[1] *Dept. Astrophysical & Planetary Sciences, University of Colorado – Boulder, Boulder, CO 80309, USA*
[2] *Laboratory for Atmospheric and Space Physics, Boulder, CO 80303, USA*
[3] *Department of Physics and Astronomy, Bates College, Lewiston, ME 04240, USA*
[4] *University of Sydney School of Mathematics and Statistics, Sydney, NSW 2006, Australia*

(Received September 27, 2018; Revised ??; Accepted ??)

Submitted to ApJ

ABSTRACT

The Rossby number is a crucial parameter describing the degree of rotational constraint on the convective dynamics in stars and planets. However, it is not an input to computational models of convection but must be measured ex post facto. Here, we report the discovery of a new quantity, the Predictive Rossby number, which is both tightly correlated with the Rossby number and specified in terms of common inputs to numerical models. The Predictive Rossby number can be specified independeint of Rayleigh number, allowing suites of numerical solutions to separate the degree of rotational constraint from the strength of the driving convection. We examine the scaling of convective transport in terms of the Nusselt number and the degree of turbulence in terms of the Reynolds number of the flow. Finally, we describe the boundary layers as a function of increasing turbulence at constant Rossby number.

Keywords: convection — rotation — turbulence

1. INTRODUCTION

Rotation influences the dynamics of convective flows in stellar and planetary atmospheres. Many studies on the fundamental nature of rotating convection in both laboratory and numerical settings have provided great insight into the properties of convection in both the rapidly rotating regime (Julien et al. 2012; Stellmach et al. 2014; Gastine et al. 2016) and the rotationally unconstrained regime (King et al. 2009; Zhong et al. 2009; Cheng et al. 2015). The scaling behavior of heat transport, the nature of convective flow structures, and the importance of boundary layers in driving dynamics are well known, and yet we are not aware of a well-developed procedure for specifying the significance of rotation on the evolved convective flows in the experimental initial conditions. The importance of rotation on convective dynamics, measured by the evolved Rossby number (Ro, the ratio of convective to rotational vorticity), is in general not held constant in parameter space studies and is often not reported.

In the astrophysical context, many studies of rotating convection have investigated questions inspired by the solar dynamo (Glatzmaier & Gilman 1982; Busse 2002; Brown et al. 2008, 2010, 2011; Augustson et al. 2012; Guerrero et al. 2013; Käpylä et al. 2014). Even when these simulations nominally rotate at the solar rate, they frequently produce distinctly different behaviors than the true Sun, such as anti-solar differential rotation profiles. These differences may arise from the fact that Ro in these simulations differs from its value the Sun. Recent simulations and experiments predict that Ro in the deep solar interior is very small, implying that deep solar convection is highly rotationally constrained, and this likely drastically affects the behavior of solar convection (Featherstone & Hindman 2016; Greer et al. 2016). In the planetary context, the balance between Lorentz and rotational forces likely leads to the observed differences between ice giant and gas giant dynamos in our solar system (Soderlund et al. 2015). In particular, Aurnou & King (2017) suggest that many studies of

Corresponding author: Evan H. Anders
evan.anders@colorado.edu

planetary systems have over-emphasized the importance of magnetism compared to rotation.

In short, simulations must have flows at the proper Rossby number if they are to explain the behavior of astrophysical objects. Here, we demonstrate an empirically derived method of *specifying* the Rossby number of convection in a simplified system. In Anders & Brown (2017) (hereafter AB17), we studied non-rotating compressible convection without magnetic fields in polytropic atmospheres. In this work, we extend AB17to rotationally-influenced, f-plane atmospheres (e.g. Brummell et al. 1996, 1998; Calkins et al. 2015). We determine how the input parameters we studied previously, controlling the Mach and Reynolds numbers of the evolved flows, couple with the the Taylor number (Ta, Julien et al. (1996)), which sets the magnitude of the rotational vector.

In section 2, we describe our experiment and paths through parameter space. In section 3, we present the results of our experiments and in section 4 we offer concluding remarks.

2. EXPERIMENT

We study fully compressible, stratified convection under precisely the same atmospheric model as we previously did in AB17, but here we have included rotation. We study polytropic atmospheres with $n_\rho = 3$ density scale heights and a superadiabatic excess of $\epsilon = 10^{-4}$ such that flows are at low Mach number. We study a domain in which the gravity, $\boldsymbol{g} = -g\hat{z}$, and rotational vector, $\boldsymbol{\Omega} = \Omega\hat{z}$, are antiparallel (Julien et al. 1996; Brummell et al. 1996).

We evolve the velocity ($\boldsymbol{u}$), temperature (T), and log density ($\ln\rho$) in the same form presented in AB17, with the addition of the Coriolis term, $2\boldsymbol{\Omega}\times\boldsymbol{u}$, to the left-hand side of the momentum equation. We impose impenetrable, stress-free, fixed-temperature boundary conditions at the top and bottom of the domain.

The kinematic viscosity (ν), thermal diffusivity (χ), and strength of rotation (Ω) are set at the top of the domain by the Rayleigh number (Ra), Prandtl number (Pr), and Taylor number (Ta),

$$\mathrm{Ra} = \frac{gL_z^3\Delta S/c_P}{\nu\chi},\ \ \mathrm{Pr} = \frac{\nu}{\chi},\ \ \mathrm{Ta} = \left(\frac{2\Omega L_z^2}{\nu}\right)^2, \quad (1)$$

where L_z is the depth of the domain, $\Delta S = \epsilon n_\rho/m$ is the specific entropy difference between $z = 0$ and $z = L_z$, and the specific heat at constant pressure is c_P. Throughout this work we set $\mathrm{Pr} = 1$.

As Ta increases, the wavenumber of convective onset, k_{crit}, also increases (Calkins et al. 2015). We study 3D Cartesian convective domains with horizontal extents of $x, y = [0, 4(2\pi/k_{\mathrm{crit}})]$. We evolve our simulations using the Dedalus[1] pseudospectral framework, and our numerical methods are identical to those presented in AB17.

As Ta increases, the critical value of Ra at which convection onsets, $\mathrm{Ra}_{\mathrm{crit}}$, also increases (see the black line in figure 1a). The linked nature of these crucial control parameters makes it difficult to predict the rotational constraint of the evolved fluid flows for a given set of input parameters. We will explore three paths through Ra-Ta space:

$$\mathrm{Ra} = \begin{cases} \mathcal{S}\,\mathrm{Ra}_{\mathrm{crit}}(\mathrm{Ta}), & \text{(I)} \\ \mathrm{Co}^2\mathrm{Pr\ Ta}, & \text{(II)} \\ \mathcal{P}_{\mathrm{Ro}}{}^2\mathrm{Pr\ Ta}^{3/4} & \text{(III)}. \end{cases} \quad (2)$$

Paths on constraint I are at constant supercriticality, $\mathcal{S} \equiv \mathrm{Ra}/\mathrm{Ra}_{\mathrm{crit}}$ (blue dash-dot line in figure 1a). Paths on constraint II are at a constant value of the classic "Convective Rossby number" ($\mathrm{Co}^2 = \mathrm{Ra}$ / [Pr Ta]), which has been used frequently in past work, and is intended to predict the Rossby number of the evolved solution (green dashed line in figure 1a; Julien et al. (1996); Brummell et al. (1996)). Paths on constraint III set constant a ratio which we call the "Predictive Rossby Number," $\mathcal{P}_{\mathrm{Ro}}{}^2 = \mathrm{Ra}/(\mathrm{PrTa}^{3/4})$, (e.g., orange solid line in figure 1a). To our knowledge, these paths have not been reported in the literature.

For each path defined in equation 2, our goal is to study the magnitude, and variation as a function of Ta, of the Rossby number,

$$\mathrm{Ro} = \frac{|\nabla\times\boldsymbol{u}|}{2\Omega}, \quad (3)$$

which quantifies the degree to which the fluid is rotationally constrained.

3. RESULTS

In figure 1a, the value of $\mathrm{Ra}_{\mathrm{crit}}$ is shown as a function of Ta, as calculated by a linear instability analysis. A sample path for each criterion in equation 2 through this parameter space is shown. In figure 1b, we display the scaling of Ro with increasing Ra along various paths through parameter space. We find that Ro increases on constant Co paths, decreases on constant $\mathcal{S}$ paths, and remains roughly constant along constant $\mathcal{P}_{\mathrm{Ro}}$ paths. In figure 1c, the behavior of Ro is shown as a function of $\mathcal{P}_{\mathrm{Ro}}$ at constant $\mathcal{S}$. At low Ro and $\mathcal{P}_{\mathrm{Ro}}$, in the rotationally constrained regime, the two parameters follow a scaling of $\mathrm{Ro} \propto \mathcal{P}_{\mathrm{Ro}}{}^{2.52}$. At higher Ro in the rotationally unconstrained regime, this scaling breaks down to

[1] http://dedalus-project.org/

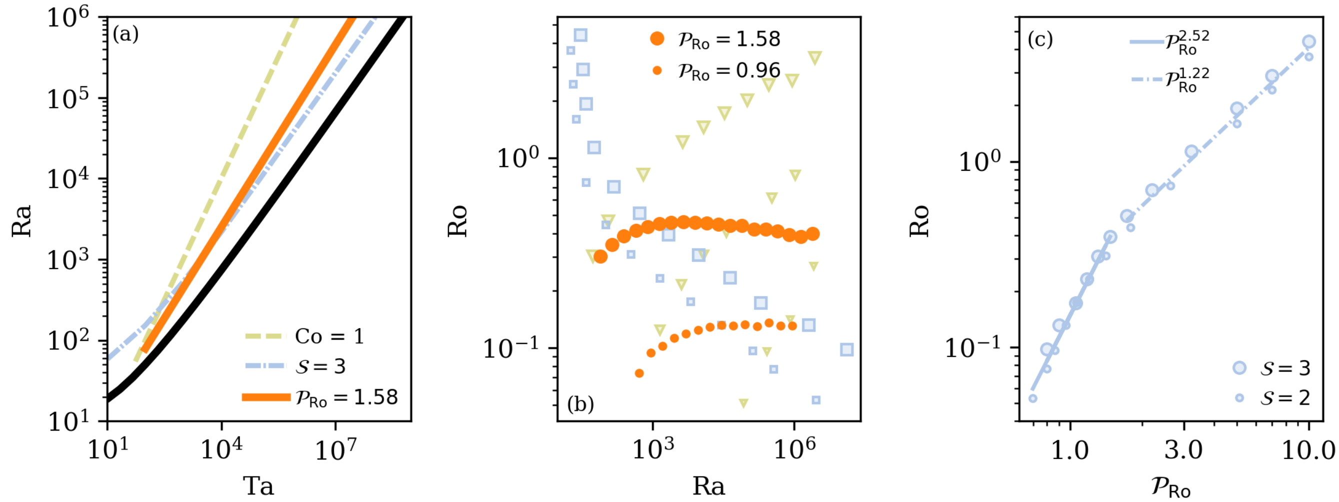

Figure 1. (a) The critical Rayleigh number, as a function of the Taylor number, is plotted as a solid black line. Paths of constant Convective Rossby Number (Co, green dashed line), constant supercriticality ($\mathcal{S}$, blue dash-dot line), and $\mathcal{P}_{\rm Ro}$ (orange solid line) are shown through parameter space. (b) Evolved Ro is plotted vs. Ra along multiple constant $\mathcal{P}_{\rm Ro}$ paths. For comparison, paths of constant $\mathcal{S}$ (blue squares; $\mathcal{S} = 3$ for big squares and $\mathcal{S} = 2$ for small squares) and constant Co (green triangles; Co = 1 for big triangles, Co = 0.3 for medium triangles, and Co = 0.1 for small triangles) are shown. Ro is roughly constant for a constant $\mathcal{P}_{\rm Ro}$, but changes drastically at constant Co and $\mathcal{S}$. (c) The scaling of Ro with $\mathcal{P}_{\rm Ro}$ is shown for $\mathcal{S} = (2, 3)$. At low Ro, both supercriticalities collapse onto a common scaling law of [NEED LAW]. At higher Ro, a different scaling law of [NEED LAW] is seen, and different supercriticalities shift Ro.

a Ro $\propto \mathcal{P}_{\rm Ro}{}^{1.22}$ law, with some offset at different values of $\mathcal{S}$.

In figure 2, sample snapshots of the evolved entropy field in the $x-y$ plane near the top of the domain are shown. In the left panel is a rotationally unconstrained flow at moderately high Ro, and Ro decreases into the rotationally constrained regime from left to right. As Ro decreases, the classic granular structure of convection (see e.g., figure 2 in AB17) gives way to vortical columns of convection, as seen in rapidly rotating Rayleigh-Bénard convection (Stellmach et al. 2014). The select cases displayed in figure 2 have an evolved volume-averaged Re $\sim$ 200.

We measure the Nusselt number (Nu), which quantifies heat transport in a convective solution, as we did in AB17. In figure 3a, we show how Nu scales as a function of Ra at fixed $\mathcal{P}_{\rm Ro}$. When Ro ~ 0.1, we find a scaling of Nu $\propto$ Ra$^{0.27}$. This is reminiscent of classic scaling laws (e.g., Ra$^{2/7}$) in non-rotating Rayleigh-Bénard convection (Ahlers et al. 2009). This suggests that changes in heat transport at constant $\mathcal{P}_{\rm Ro}$ are driven by changes in the boundary layer structure with increasing Ra. In figure 3b, we plot the RMS Reynold's number (Re $= |u|L_z/\nu$) as a function of Ra at fixed $\mathcal{P}_{\rm Ro}$, and find that Re $\propto$ Ra$^{0.47} \sim$ Ra$^{1/2}$ in the rotationally constrained regime, which directly parallels [WHAT DOES "DIRECTLY PARALLELS" MEAN?] the non-rotating regime in AB17.

Figure 4 shows time- and horizontally-averaged profiles of Ro and the entropy gradient (∇s [SEE JSO COMMENT IN CAPTION]). As Ra increases at a constant value of $\mathcal{P}_{\rm Ro}$, both the ∇s and Ro boundary layers become thinner. We measure the thickness of the entropy boundary layer ($\delta_{\nabla s}$) at the top of the domain by measuring where a linear fit within the boundary layer crosses through $\nabla s = 0$. We ensure by-eye for each profile that this is a reasonable measure of the boundary layer thickness. We measure the thickness of the Ro boundary layer ($\delta_{\rm Ro}$) as the height of the peak value of Ro within the upper half of the domain. In figure 4e, we plot $\delta_{\rm Ro}/\delta_{\nabla s}$, the ratio of these two boundary layers. As anticipated, the dynamical boundary layer ($\delta_{\rm Ro}$) becomes relatively thinner with respect to the thermal boundary layer ($\delta_{\nabla s}$) as Ro and $\mathcal{P}_{\rm Ro}$ decrease. [need a sentence saying what this means?]

4. DISCUSSION

In this letter, we studied low-Mach-number, stratified, compressible convection under the influence of rotation. We examined three paths through Ra-Ta space, and showed that in the rotationally constrained regime at low-Ro, the newly-defined Predictive Rossby number, $\mathcal{P}_{\rm Ro} = \text{Ra}/(\text{Pr Ta}^{3/4})$, determines the value of the evolved Ro. While increasing Ra and holding $\mathcal{P}_{\rm Ro}$ constant, we find scaling laws of heat transport (Nu) and

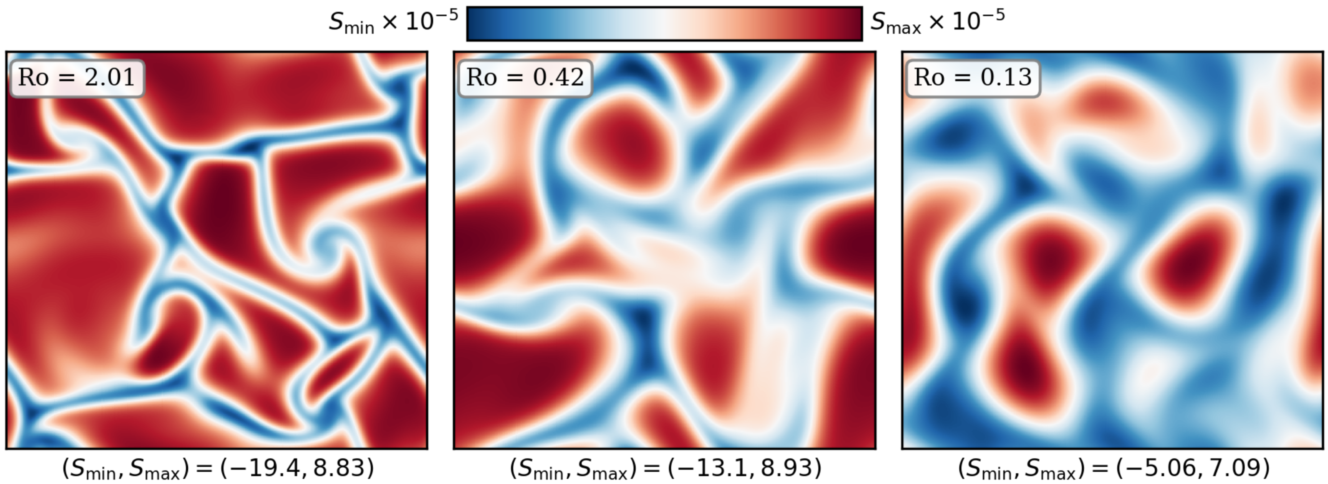

Figure 2. A horizontal slice of the evolved entropy field is plotted at $z = 0.95L_z$ for select simulations. The mean value of entropy at this height has been removed in all cases. All runs displayed here have an evolved volume-averaged Re$\sim$ 200. As Ro decreases from O(1) on the left to O(0.1) on the right, and thus the rotational constraint on the flow increases, significant changes in flow morphology are observed. At Ro = 2.01, convective dynamics are not hugely dissimilar from the non-rotating case where there are large upflows and narrow, fast downflow lanes (see e.g., AB17). As the rotational constraint increases, the granular convective pattern gives way to vortical columns, as seen at Ro = 0.13.

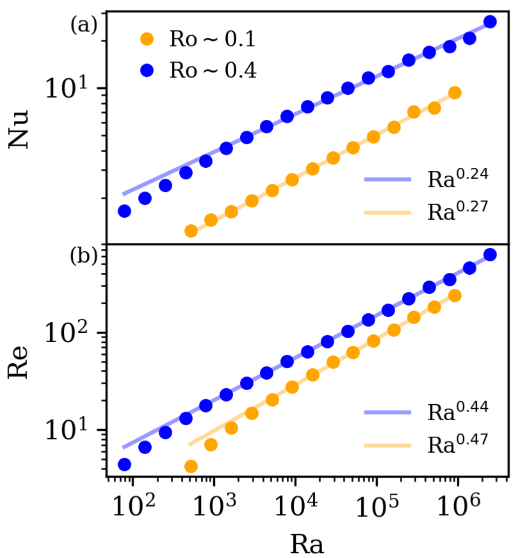

Figure 3. Scaling laws for paths at $\mathcal{P}_{\rm Ro} = 1.58$ (Ro $\sim$ 0.4) and $\mathcal{P}_{\rm Ro} = 0.96$ (Ro $\sim$ 0.1) are shown. (a) Evolved Nu vs. Ra. The scaling laws here are very reminiscent of classic Rayleigh-Bénard convection theory (Ahlers et al. 2009). (b) Evolved Re vs. Ra. The scaling seen here is nearly identical to scalings in nonrotating convection.

turbulence (Re) that are nearly identical to scaling laws seen in nonrotational convection.

Our results suggest that by choosing the proper value of $\mathcal{P}_{\rm Ro}$, experimenters can can select the degree of rotational constraint present in their simulations. Once that value is chosen, it is straightforward to increase the turbulent nature of the simulations by increasing Ra, just as in the non-rotating case. Although all the results reported here are for a simple Cartesian geometry with antiparallel gravity and rotation, preliminary 3D spherical simulations suggest that tthey are applicable to rotating convection in those geometries as well (Brown et al. 2019 in prep).

EHA acknowledges the support of NASA NESSF (insert fellowship number) and the University of Colorado's George Ellery Hale Graduate Student Fellowship. This work was additionally supported by NASA LWS grant number NNX16AC92G. Computations were conducted with support by the NASA High End Computing (HEC) Program through the NASA Advanced Supercomputing (NAS) Division at Ames Research Center on Pleiades with allocations GID s1647.

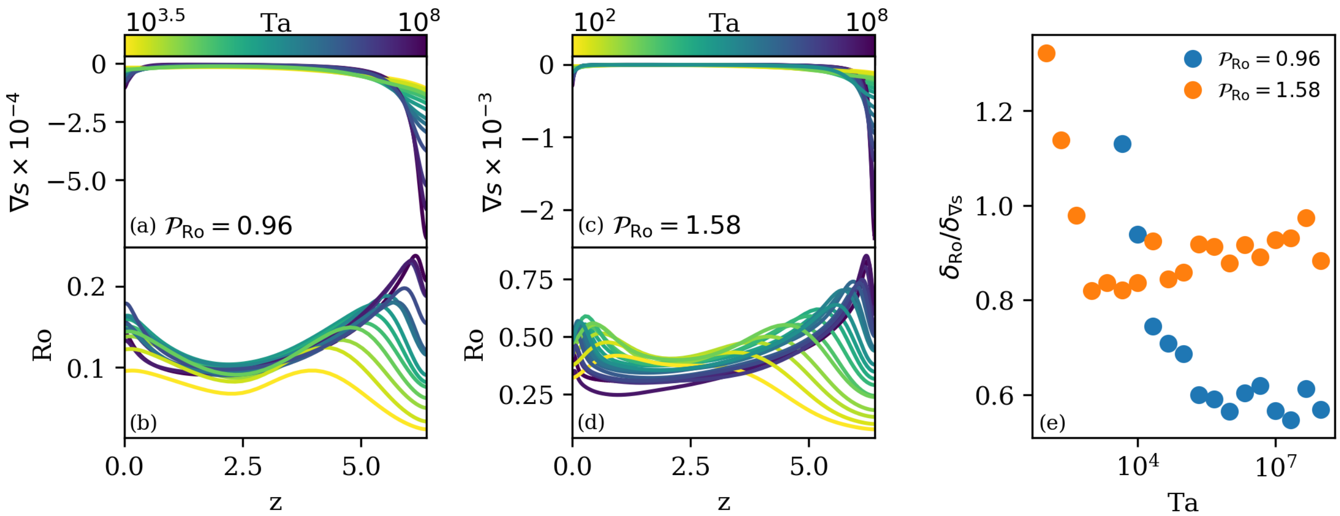

Figure 4. Horizontally-averaged profiles of the magnitude of [OR z component as is accurate] the entropy gradient ($|\nabla s|$ [or $(\nabla s)_z$], a) and Rossby number (Ro, b) are shown vs. height for $\mathcal{P}_{\rm Ro} = 0.96$. Similar profiles are shown in (c) and (d) for $\mathcal{P}_{\rm Ro} = 1.58$. (c) The ratio of the sizes of the Ro boundary layer and ∇s boundary layer are shown. We find that for increasingly rotationally constrained flows, the Ro boundary layer is increasingly thinner than the thermal boundary layer.

REFERENCES

Ahlers, G., Grossmann, S., & Lohse, D. 2009, Rev. Mod. Phys., 81, 503

Anders, E. H., & Brown, B. P. 2017, Physical Review Fluids, 2, 083501

Augustson, K. C., Brown, B. P., Brun, A. S., Miesch, M. S., & Toomre, J. 2012, ApJ, 756, 169

Aurnou, J. M., & King, E. M. 2017, Proceedings of the Royal Society of London Series A, 473, 20160731

Brown, B. P., Browning, M. K., Brun, A. S., Miesch, M. S., & Toomre, J. 2008, ApJ, 689, 1354

—. 2010, ApJ, 711, 424

Brown, B. P., Miesch, M. S., Browning, M. K., Brun, A. S., & Toomre, J. 2011, ApJ, 731, 69

Brummell, N. H., Hurlburt, N. E., & Toomre, J. 1996, ApJ, 473, 494

—. 1998, ApJ, 493, 955

Busse, F. H. 2002, Physics of Fluids, 14, 1301

Calkins, M. A., Julien, K., & Marti, P. 2015, Geophysical and Astrophysical Fluid Dynamics, 109, 422

Cheng, J. S., Stellmach, S., Ribeiro, A., et al. 2015, Geophysical Journal International, 201, 1

Featherstone, N. A., & Hindman, B. W. 2016, ApJ, 830, L15

Gastine, T., Wicht, J., & Aubert, J. 2016, Journal of Fluid Mechanics, 808, 690

Glatzmaier, G. A., & Gilman, P. A. 1982, ApJ, 256, 316

Greer, B. J., Hindman, B. W., & Toomre, J. 2016, ApJ, 824, 4

Guerrero, G., Smolarkiewicz, P. K., Kosovichev, A. G., & Mansour, N. N. 2013, ApJ, 779, 176

Julien, K., Knobloch, E., Rubio, A. M., & Vasil, G. M. 2012, Physical Review Letters, 109, 254503

Julien, K., Legg, S., McWilliams, J., & Werne, J. 1996, Journal of Fluid Mechanics, 322, 243

Käpylä, P. J., Käpylä, M. J., & Brandenburg, A. 2014, A&A, 570, A43

King, E. M., Stellmach, S., Noir, J., Hansen, U., & Aurnou, J. M. 2009, Nature, 457, 301

Soderlund, K. M., Sheyko, A., King, E. M., & Aurnou, J. M. 2015, Progress in Earth and Planetary Science, 2, 24

Stellmach, S., Lischper, M., Julien, K., et al. 2014, PhRvL, 113, 254501

Zhong, J.-Q., Stevens, R. J. A. M., Clercx, H. J. H., et al. 2009, Physical Review Letters, 102, 044502